JOURNAL OF Materials CHEMISTRY

Synthesis and characterization of crystalline tin oxide nanoparticles

Sophie de Monredon,[a] Antoine Cellot,[a] François Ribot,*[a] Clément Sanchez,[a] Lidia Armelao,[c] Lethicia Gueneau[c] and Laurent Delattre[c]

[a]*Laboratoire de Chimie de la Matière Condensée, UMR CNRS 7574, Université Pierre et Marie Curie, 4 place Jussieu, 75252 Paris cedex 05, France. E-mail: fri@ccr.jussieu.fr*
[b]*Dipartimento di Chimica Inorganica Metallorganica ed Analitica, Universita degli Studi di Padova, 1 via Marzolo, 35131 Padova, Italy*
[c]*Saint-Gobain Recherche, 39 quai Lucien Lefranc, BP 135 93303 Aubervilliers cedex, France*

Received 26th March 2002, Accepted 22nd May 2002
First published as an Advance Article on the web 28th June 2002

Monodisperse non-aggregated spheroidal nanoparticles of SnO_2 cassiterite are prepared through hydrolysis of tin isopropoxide in the presence of acetylacetone and *p*-toluenesulfonic acid, followed by ageing at 60 °C. The obtained sols remain stable for several months at 4 °C. The nanoparticles have been characterized in the solid state (xerosol) by powder X-ray diffraction, TEM, FTIR, TGA-DTA, and ^{119}Sn MAS and ^{13}C CP-MAS NMR. The mean size of the cassiterite oxide core is about 1–2 nm. These particles do not aggregate in suspension because their surfaces are protected by an hybrid organic–inorganic layer containing acetylacetonate ligands, acetylacetone, *p*-toluenesulfonates and water.

Introduction

Crystalline tin oxide, cassiterite structure, is a wide band gap semiconductor (~3.6 eV), which, in its as-grown state, is typically n-type. Because of its optical (transparent for visible light and reflective for IR) and electrical properties, allied to good chemical and mechanical stability,[1] it can be used, often doped with antimony or fluoride, in many applications, such as transparent conductive electrodes,[2–6] photovoltaic devices,[7,8] photosensors,[9] catalysis[10] and antistatic coatings.[11–13] However, its most important use is as the active layer in gas-sensing devices, for which measurement of the electrical conductivity allows the concentration of inflammable and/or toxic gases (H_2, CO, CH_4, ···) to be monitored.[14–19] In such an application, reducing the size of the particles, down to a few nanometers, is of interest since the sensitivity of the sensors can be greatly increased as a result of the associated increase of the active surface where oxygen adsorption/desorption can take place.[15,16,20,21]

Tin oxide-based materials have been prepared by many different techniques; some involve dry processes, such as sputtering from a tin oxide target[22,23] or from a metallic target followed by oxidation,[24] laser ablation[15] and chemical vapor deposition (CVD),[25] others are based on wet processes, including spray pyrolysis,[26–28] decomposition/oxidation of tin(II) amides[29] and sol–gel-related methods, which have been used to prepare tin oxide coatings, particles and precipitates.[4,6,30–42]

Among the different possible synthetic outcomes, stable sols of crystalline tin oxide nanoparticles are of interest for the preparation of antistatic coatings,[13] conductive coatings,[4] filtration membranes[4] and gas sensors.[29] Indeed, the sol state can be easily used for dip- or spin-coatings. Moreover, the already crystalline nature of the particles can likely reduce the thermal treatment generally needed in the preparation of such materials. One key point in the synthesis of nanoparticles is the control of their growth and agglomeration by poisoning their surfaces, *e.g.* by using a complexing ligand.[4,29,43–46]

The sol–gel process is known as a way to prepare dispersed materials through the growth of metal oxo-polymers in a solvent.[47,48] The chemistry involved in the sol–gel process is based on the inorganic polymerization of molecular precursors such as metal alkoxides, $M(OR)_n$, and sol, gels or precipitates can be obtained depending on the chemical conditions which control the growth and branching of the forming oxo-polymers.[49] For all metallic elements (transition, main group, rare earth) but silicon, the reactions involved, *i.e.* hydrolysis and condensation, are generally fast and need to be inhibited to avoid precipitation and allow sol or gel formation. Such control can be classically achieved by the use of strong complexing ligands, such as carboxylic acids, ß-diketones and allied derivatives, which readily react with metal alkoxides to form modified precursors of differentiated reactivity.[42–44,50–56] The complexing ligands also act as surface poisons and allow, in some cases, the formation of fairly well-defined nanoparticles.[43–45] Moreover, hydrolysis with water acidified with a poorly complexing acid (*e.g. p*-toluenesulfonic acid), accompanied by mild thermal treatment, allows easier redistribution of the M–O–M bonds and favors the crystallization of the nanoparticles.[43,44]

Such an approach has been used in this work, which describes the synthesis of monodisperse non-aggregated particles of SnO_2 cassiterite with a mean size of about 2 nm. Moreover, the resulting sols are stable for 3 months at 4 °C, improving the processability of these nanomaterials. The tin oxide nanoparticles have been characterized in the solid state by using X-ray diffraction, TEM, FTIR, TG-DTA, and ^{119}Sn MAS and ^{13}C CP-MAS NMR.

Experimental

Preparation of the sols

Tin isopropoxide [$Sn(O^iPr)_4$.^{i}PrOH, Gelest] was dissolved in absolute ethanol under a dry atmosphere (10 g of ethanol was used per 1 g of tin isopropoxide). 2,4-Pentanedione (acetylacetone, acacH) was added, through a septum and under magnetic stirring, to achieve complexant/metal ratios (A = acacH/Sn) ranging from 2 to 6. Then, hydrolysis was performed, under magnetic stirring, with acidic aqueous solutions (*p*-toluenesulfonic acid, HPTS) in order that the initial hydrolysis ratio ($H = H_2O/Sn$) was always 10, but with acidity ratios (R = HPTS/Sn) ranging from 0 to 0.6. After stirring at room temperature for 2 h, these solutions were aged

 DOI: 10.1039/b203049g

Table 1 Synthesis parameters for xerosols P_X

Xerosol	A (= acacH/Sn)	R (= H^+/Sn)	Ageing temp./°C	Ageing time/h
P_2	0	0.4	60	24
P_3	0	0.0	60	24
P_4	5	0.0	60	24
P_5	5	0.4	60[a]	24
P_6	5	0.4	—	—
P_7	0	0.0	—	—
P_8	5	0.4	78[b]	24
P_9	5	0.4	78[b]	48

[a]HCl was used instead of HPTS. [b]solution reflux

for 24 h in tightly sealed glass bottles inside an oven (60 °C). Some experiments were aged for a longer time (48, 72 h) or at a higher temperature (~78 °C, reflux in a round-bottom flask equipped with a condenser). In the final sols, the concentrations of tin were about 0.25 mol L^{-1}. The most studied sols are labelled S_A and the synthesis conditions correspond to variable A, $H = 10$, $R = 0.4$, 60 °C and 24 h.

Preparation of the xerosols

The xerosols were obtained by drying the sols at 60 °C under reduced pressure. The xerosols X_A derive from the sols S_A. For comparative purposes, a series of additional xerosols, labelled P_X, was also prepared. Their synthesis parameters are reported in Table 1. To check their evolution under thermal treatment, some xerosols were also heat treated (for 2 h) in a tubular furnace under oxygen at 150, 300, 450, 750 or 1000 °C.

Characterization techniques

Transmission electron microscopy (TEM) was performed with a Jeol 100 CXII (100 or 120 kV) microscope. The sols were diluted (*ca.* 500 times in ethanol) and a drop was deposited onto a carbon-coated grid.

FT infrared spectra were recorded on a Nicolet Magna 550 spectrometer (32 scans at a resolution of 4 cm^{-1}). The xerosols were pelleted with dried KBr and analyzed in transmission mode.

Simultaneous thermogravimetry and differential thermal analysis (TG-DTA) were carried out with a TA Instruments SDT 2960 analyser. Experiments were carried out under oxygen (100 cm^3 min^{-1}) with heating rates of 2 or 10 °C min^{-1}.

X-Ray diffraction (XRD) patterns were obtained with a Philips PW1830 powder diffractometer working with Cu-Kα radiation and operating in reflection geometry with a graphite back monochromator. The patterns were recorded from 2 to 80° (2θ) in steps of 0.05° with a counting time of 40 s per point. The position and width of the lines were determined using the "Fit Profile" subroutine of the Philips APD 3.5 program package. The average crystallite size was deduced from the half-height line broadening by applying the Scherrer formula and assuming Gaussian profiles for experimental and instrumental broadenings.[57]

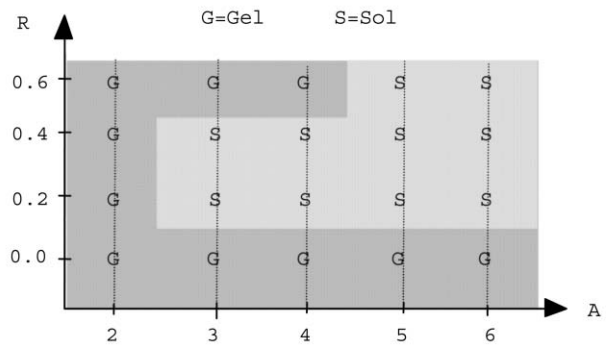

Fig. 1 Outcomes of the synthesis for different complexation ratios (A = acac/Sn) and acidity ratios (R = HPTS/Sn). The hydrolysis conditions were $H = 10$, 60 °C and 24 h in all cases.

^{119}Sn MAS and ^{13}C CP-MAS solid state NMR spectra were recorded on a Bruker MSL300 spectrometer (300.13, 75.47 and 111.89 MHz for ^{1}H, ^{13}C and ^{119}Sn, respectively) equipped with a 4 mm high-speed locked Bruker probe. ^{119}Sn MAS NMR spectra were obtained at 13 kH, with a pulse of 1.5 μs (*ca.* 30°) and a recycling delay of 15 s. ^{119}Sn isotropic chemical shifts are referenced to tetramethyltin using tetracyclohexyltin as a secondary external reference ($\delta = -97.35$ ppm).[58] The accuracy on the chemical shift is ±1 ppm. The spectra were deconvoluted with WinFit software.[59] The ^{13}C CP-MAS NMR spectra were obtained at 10 kHz with a 90° pulse of 4 μs, a contact time of 1 ms and a recycling delay of 5 s. Even though not optimum for the polarization transfer, a speed of 10 kHz was chosen to avoid overlaps between isotropic resonances and spinning side bands. 1000 Transients were summed for each sample. ^{13}C isotropic chemical shifts are referenced to tetramethylsilane.

Results and discussion

Influence of the synthesis parameters

The complexant/metal ratio (A = acac/Sn) and the acidity ratio (R = HPTS/Sn) were systematically varied. *p*-Toluenesulfonic acid was chosen, according to previous works on other tetravalent metals (Ti, Zr), mainly because *p*-toluenesulfonate is a poor complexant.[43,44] Fig. 1 summarizes the results obtained after 24 h at 60 °C; colloidal solutions (sols) or opalescent gels are the observed outcomes. Gels are formed when no acid is added, whatever the complexant ratio, or when $A = 2$, whatever the acidity ratio. Addition of excessive amounts of acid ($R = 0.6$) also shifts the gel–sol border towards higher complexant ratios. For $A = 5$ and $R = 0.4$, ageing time and temperature were also varied. After 48 h of ageing at 60 °C, the system remains a sol, but turns into a gel after 72 h of ageing. Raising the temperature to *ca.* 78 °C (reflux conditions) does not modify the outcome.

Controlling the hydrolysis-condensation of a metal alkoxide by adding a strong complexing ligand (SCL) and/or raising the acidity is a well-known method.[32,42–45,50–56] The addition of the ligand causes the formation of new precursors, $M(OR)_{n-x}(SCL)_x$, in which the new ligands are less hydrolyzable. For tin isopropoxide and acetylacetone, the new precursor is $Sn(OPr^i)_2(acac)_2$, as the complexing ratios used are always greater than 2;[42,55,60–62] $Sn(acac)_4$ is never observed because of steric hindrance.[61] In the control of the growth of the oxo-polymer, the ligands also act as a protective coating on the surface of the particles and prevent them from aggregating.[43,44,46] Compared to other tetravalent metals (Ti^{IV}, Zr^{IV}, Ce^{IV}), tin needs a higher amount of acetylacetone to avoid the formation of gels. This feature is likely related to the lower stability towards hydrolysis of the Sn–acac bond. Therefore, large amounts of free acetylacetone are necessary to displace the hydrolysis–complexation equilibrium and maintain enough acetylacetonate bound to tin. However, the presence of protons also appears necessary. Protons likely slow down hydrolysis by making H_2O a worse electrophile.[56] However, a high acidity ratio can also favour the protonation of acetylacetonate and ease the cleavage of M–acac bonds. Indeed, for $R = 0.6$, a complexation ratio of 5 is necessary to avoid gelation.

Thermal ageing (60 or 78 °C) appears necessary to generate crystalline nanoparticles (*vide infra*), yet extended thermal ageing times (72 h) lead to gels. Indeed, the formed sols are only kinetically stable. They turn into gels after few weeks at room temperature, but can be kept intact for several months when stored at 4 °C.

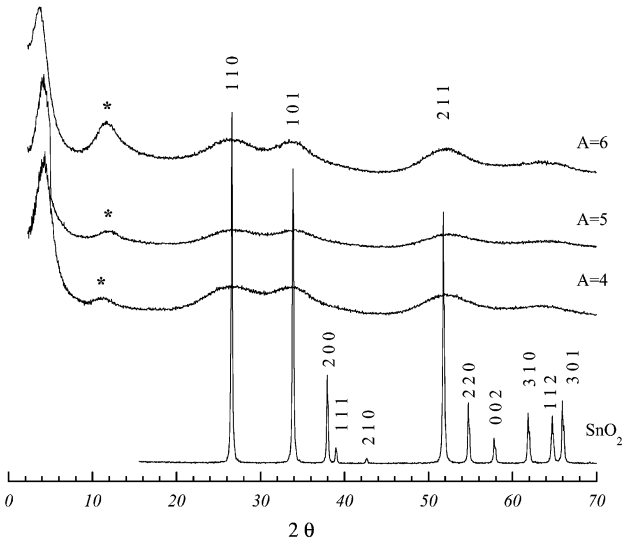

Fig. 2 Powder X-ray diffraction patterns of xerosols X_4, X_5, X_6 and crystalline SnO_2 with a large grain size. The indexation corresponds to cassiterite (peaks marked with an asterisk are related to the sample holder).

Characterization of the xerosols

XRD–TEM. Fig. 2 shows the typical XRD patterns recorded for all our xerosols. These patterns are characteristic of crystalline particles of SnO_2 cassiterite.[63] The mean size of the crystallites, assuming a line broadening essentially due to the size effect, has been determined between 12 and 18 Å. In contrast to titanium,[43] no clear effect of the complexation ratio has been observed on the mean size. The different ageing temperatures (60 or 78 °C) and times (24 or 48 h) give identical results. The diffractogram of P_6 (no thermal ageing) does not exhibit any crystalline features, clearly showing that thermal ageing is necessary to promote crystallization. The increased temperature likely favors the proton-assisted reorganization of the Sn–O–Sn framework.

The mean sizes obtained by XRD on xerosols are consistent with the TEM images (Fig. 3) of sols which show an homogeneous dispersion of spheroidal particles with diameters ranging from 1 to 2 nm. Lattice planes can also be observed in the particles. Electron diffraction experiments confirm the cassiterite structure and indicate that the observed planes correspond to a 101 orientation (d_{101} = 2.65 Å).[63] The crystallites evidenced by XRD are therefore the constituent particles of the sols.

The XRD patterns also exhibit an intense and narrow peak at low angles ($2\theta \approx 4°$, $d \approx 25$ Å), which indicates a good degree of organization in the particles packing, evidencing the monodispersity of the nanoparticles. The difference between this packing distance and the crystallite size, *ca.* 10 Å, is likely due to the amorphous layer and adsorbed species which surround the particles (*vide infra*).

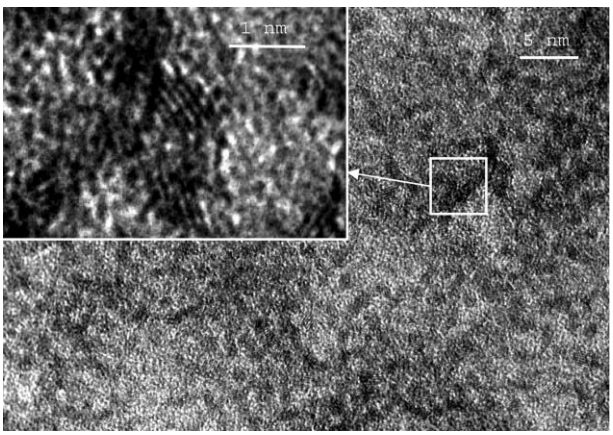

Fig. 3 TEM images of S_5.

FT-IR spectroscopy. The infrared spectra of the xerosols exhibit a strong vibration extending from 3600 to 2500 cm^{-1}, which indicates the presence of hydrogen bonds involved in O–H oscillators.[64,65] These vibrations arise from SnOH groups and adsorbed water molecules.[41] The spectra also display bands at 1570 and 1540 cm^{-1} corresponding to the enol form of acetylacetonato groups bonded to tin.[64] No evidence for free acetylacetone (ketone-related vibrations) or ethanol is found in the spectra, showing that the drying step is efficient. The low wavenumber region exhibits a strong vibration around 600 cm^{-1}, which can be assigned to ν(Sn–O–Sn) of the tin oxide framework.[41] Four vibrations (1210, 1125, 1040 and 1014 cm^{-1}) characteristic of HPTS are also observed, indicating the presence of HPTS that cannot be removed during the drying process.[43]

Thermal evolution of the xerosols. Four weight losses are observed on the TGA trace of X_5: the first (4.2%, RT to 150 °C, very broad phenomenon without any clear endo or exothermal character) likely corresponds to the evaporation of residual free organics (EtOH) or water; the second weight loss (7.1 %, *ca.* 250 °C, weak endo.) is related to the departure of bound acetylacetonate (*vide infra*); the third (29%, 430 °C, strong exo.) corresponds to the decomposition of *p*-toluenesulfonate groups; finally, the last weight loss (4.3%, *ca.* 550 °C) is probably due to the condensation of Sn–OH surface groups[41] and to the combustion of organics residues generated by the decomposition of *p*-toluenesulfonate. After 2 h at 150 or 300 °C, XRD does not reveal any increase in the crystallite size, which remains around 1–2 nm. This feature is likely related to the remaining organic groups (acac up to 250 °C and *p*-toluenesulfonate up to 430 °C) which still cover the surface of the nanoparticles. At higher temperatures, the crystallites start to grow (Table 2), which also causes the disappearance of the low angle peak ($2\theta \approx 4°$) related to the packing of the nanoparticles.

Table 2 ^{119}Sn MAS NMR data and crystallite sizes

Sample	δ_{iso}/ppm	Width/Hz	Proportion (%)	Size/nm[a]
X_5	−607	1800	18	1–2
	−612	4700	45	
	−660	3400	37	
X_5 @ 150 °C	−606	2000	29	1–2
	−620	4400	44	
	−659	3000	27	
X_5 @ 300 °C	−605	2500	32	1–2
	−627	8064	68	
X_5 @ 450 °C	−602	2100	100	11
X_5 @ 750 °C	−602	1800	100	11
X_5 @ 1000 °C	−603	700	100	22
P_2 (cryst.)[b]	−607	1700	36	
	−623	5000	64	
P_3 (am.)[b]	−607	6000	100	
P_4 (cryst.)[b]	−607	2200	48	
	−613	6200	52	
P_5 (cryst.)[b]	−604	4100	56	
	−616	9300	33	
	−650	2100	11	
P_6 (am.)[b]	−609	4100	17	
	−658	4600	83	
P_7 (am.)[b]	−609	6800	100	

[a]Determined by XRD. [b]cryst.: crystallized as SnO_2 cassiterite; am.: amorphous.

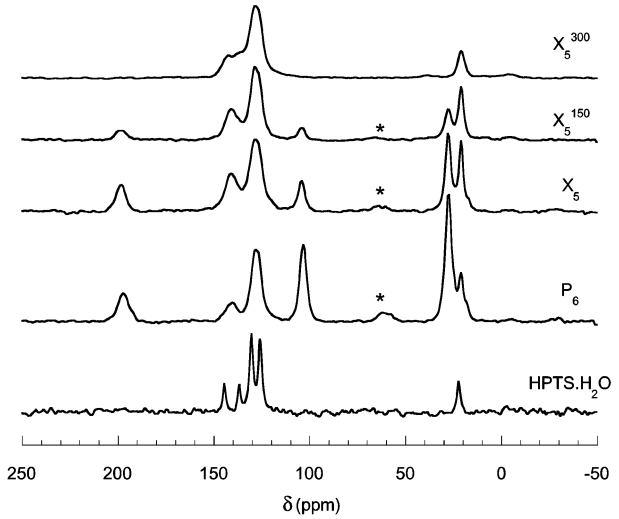

Fig. 4 ^{13}C CP-MAS NMR spectra of X_5, X_5 treated at 150 or 300 °C, P_6 and HPTS·H_2O (asterisks indicate spinning side bands).

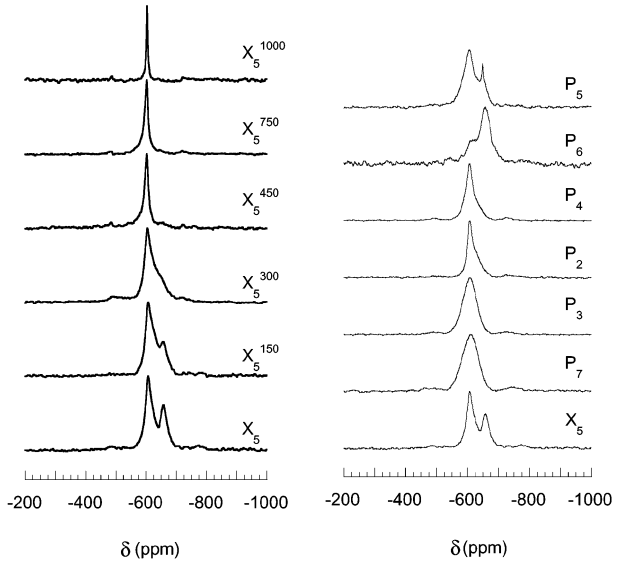

Fig. 5 ^{119}Sn MAS NMR spectra of X_5, X_5 heat treated at 150, 300, 450, 750 or 1000 °C and P_2–P_7.

Solid state NMR. Fig. 4 presents the ^{13}C CP-MAS NMR spectra of X_5, X_5 treated at 150 or 300 °C, and P_6 (same synthesis parameters as X_5, but without ageing at 60 °C). The spectrum of X_5 is representative of the other xerosols X_A. The resonances located at 141, 128 and 22 ppm correspond to the quaternary CH and CH_3 carbons of *p*-toluenesulfonate groups, respectively. The two resonances located in the aromatic region are fairly broad (*ca.* 10 ppm or 800 Hz) and no distinction can be made between the two quaternary carbons or the two CH carbons, as in HPTS·H_2O, where four resonances are clearly observed (144.5, 136.7, 130.3 and 125.8 ppm). The broadness of these resonances for the xerosols is likely due to the presence of different environments for the PTS groups. The resonances at 199, 105, and 28 ppm correspond to the carbonyl, CH and CH_3 groups of acetylacetonato ligands.[43] They completely disappear when X_5 is treated at 300 °C, indicating complete removal of the acetylacetonato ligands at this temperature, in relation to the weak endotherm at 250°C. However, a new broad signal also appears around 137 ppm and is likely related to some decomposition products of the acetylacetonato ligands. The ^{13}C CP-MAS spectrum of X_5 treated at 450 °C (not shown) conatins no signals, indicating that at this temperature most of the organic residues have been lost, in agreement with the TGA trace. Because of polarization transfer, which depends on the environment and on mobility, CP-MAS is not directly quantitative. However, due to the similarity of the products, the acac/PTS ratio in X_5 can be reasonably assumed to be smaller than in P_6. Therefore, the thermal ageing step promotes crystallization (*vide supra*) and favors the hydrolysis of acetylacetonato groups.

Fig. 5 presents the ^{119}Sn MAS NMR spectra of X_5 and X_5 treated at different temperatures (150, 300, 450, 750 and 1000 °C). The spectrum of X_5 is representative of the other xerosols. For comparison purposes, the ^{119}Sn MAS NMR spectra of products P_2 to P_7 are also presented in Fig. 5. From one to three overlapping resonances, all characteristic of hexacoordinated tin atoms, are necessary to deconvolute the spectra and the results are gathered in Table 2. The first resonance of X_5, at −607 ppm, can be assigned to the tin atoms of the crystalline core of the nanoparticles. Bulk tin oxide exhibits a ^{119}Sn chemical shift of -603 ± 2 ppm.[66] The observed difference is likely due to the very small size of the crystallites and, therefore, to surface effects. Indeed, when the samples are treated above 450 °C, the crystallite size increases and the ^{119}Sn chemical shift returns to its expected value (Table 2). Except for the sample treated at 1000 °C, there is no clear effect of the crystallite size on the resonance width, which remains around 2000 Hz for sizes ranging from 1–2 to 11 nm. This observation is somewhat different from what was reported for SnO_2 crystallites ranging from 5 to 35 nm.[40] However, only one site was considered in this study, even though the resonances were clearly dissymmetric. Therefore, a strict comparison is not obvious.

The two other resonances of X_5, at −612 and −660 ppm, are more difficult to assign. That at low frequency decreases when X_5 is treated at 150 °C and disappears after treatment at 300 °C. Therefore, this resonance is likely related to the presence of acetylacetonato ligands, for which ^{13}C NMR indicates a decrease at 150 °C and complete removal at 300 °C. Moreover, the presence of an acetylacetonato ligand on tin is indeed expected to shift the resonance to lower frequency compared to tin oxide.[42,55,60] However, sample P_4, which contains acac, does not exhibit such a resonance. This low frequency signal appears only when acac is combined with acidic hydrolysis. Consequently, the resonance around −660 ppm is assigned to surface tin atoms which simultaneously bear an acetylacetonato ligand and a protonated hydroxo ligand ($-OH_2^+$). In sample P_5, which was prepared with HCl instead of HPTS, this signal is narrower and shifted to −650 ppm. These features are likely due to the different charge compensation of the protonated hydroxo (Cl^- instead of PTS^-).

The last resonance, at −612 ppm, is less well defined. It could correspond to surface tin atoms which are not simultaneously bounded to an acetylacetonato and a protonated hydroxo group. The evolution of this third resonance among the different samples (from −612 to −627 ppm) is likely due to the ill-defined character of these surfaces sites.

Conclusion

Monodisperse spheroidal crystalline nanoparticles of tin oxide are obtained through the hydrolysis of tin isopropoxide in the presence of acetylacetone and protons, followed by ageing at 60 °C. The mean size of the cassiterite oxide core is around 1–2 nm. These nanoparticles are non-aggregated in the sol state. The protection of these particles towards aggregation is likely ensured by the complexation of the surface tin atoms by acetylacetonato ligands. The sols obtained remain stable for several months at 4 °C and can be used to proces films on glass by dip- or spin-coating.[13] A thermal treatment up to 450 °C in air appears necessary to remove the organic residue (acac and *p*-toluenesulfonate) and causes a slight increase in the

crystallite size. Such thermally treated films exhibit antistatic properties.[13] The use of these nanoparticles and derived films for gas sensing is currently under investigation.

Acknowledgement

S. de M. and A. C. are indebted to Saint Gobain Recherche for financial support.

References

1 K. L. Chopra, S. Major and D. K. Pandya, *Thin Solid Films*, 1983, **102**, 1.
2 D. S. Ginley and C. Bright, *Mater. Res. Soc. Bull.*, 2000, **25**, 15.
3 C. G. Granqvist, *Appl. Phys. A: Mater. Sci. Process.*, 1993, **57**, 19.
4 C. Goebbert, M. A. Aegerter, D. Burgard, R. Nass and H. Schmidt, *J. Mater. Chem.*, 1999, **9**, 253.
5 H. Cachet, J. Bruneaux, G. Folcher, C. Lévy-Clément, C. Vard and M. Neumann-Spallart, *Sol. Energy Mater. Sol. Cells*, 1997, **46**, 101.
6 M. A. Aegerter, A. Reich, D. Ganz, G. Gasparro, J. Pütz and T. Krajewski, *J. Non-Cryst. Solids*, 1997, **218**, 123.
7 S. Ferrere, A. Zaban and B. A. Gregg, *J. Phys. Chem. B*, 1997, **101**, 4490.
8 D. A. Gaal and J. T. Hupp, *J. Am. Chem. Soc.*, 2000, **122**, 10956.
9 J. R. Bellingham, W. A. Philips and C. J. Adkins, *J. Mater. Sci. Lett.*, 1992, **11**, 263.
10 V. C. Cebolla, R. Bacaud, M. Besson, D. Cagniant, H. Charcosset and M. Oberson, *Bull. Soc. Chim. Fr.*, 1987, 935.
11 J. C. Robert, *US Pat*., 5494652, 1996.
12 C. G. Granqvist, *Solid State Mater. Sci.*, 1990, **16**, 291.
13 A. Cellot, S. de Monredon, L. Delattre, L. Guéneau, F. Ribot and C. Sanchez, in *Proceedings of the Conference on Nanostructured Materials made from Self-Assembled Molecules and Particles, Hindås, Sweden, 7–10 Jan, 2001*.
14 Y. Shimizu and M. Egashira, *Mater. Res. Soc. Bull.*, 1999, **24**, 18.
15 G. Williams and G. S. V. Coles, *Mater. Res. Soc. Bull.*, 1999, **24**, 25.
16 G. Martinelli, M. C. Carotta, E. Traversa and G. Ghiotti, *Mater. Res. Soc. Bull.*, 1999, **24**, 30.
17 B. Panchpakesan, D. L. DeVoe, M. R. Widmaier, R. Cavicchi and S. Semancik, *Nanotechnology*, 2001, **12**, 336.
18 W. J. S. Robert, S. M. Yang, G. Chabanis, N. Coombs, D. E. Williams and G. A. Ozin, *Adv. Mater.*, 2001, **13**, 1468.
19 S. R. Davis, A. V. Chadwick and J. D. Wright, *J. Mater. Chem.*, 1998, **8**, 2065.
20 X. Wang, S. S. Yee and W. P. Carey, *Sens. Actuators, B*, 1995, **24-25**, 454.
21 G. Zhang and M. L. Liu, *Sens. Actuators, B*, 2000, **69**, 144.
22 G. Micocci, A. Serra, P. Siciliano, A. Tepore and Z. Ali-Adib, *Vacuum*, 1996, **47**, 1175.
23 C. Geoffroy, G. Campet, F. Menil, J. Portier, J. Salardenne and G. Couturier, *Act. Passive Elec. Comput.*, 1991, **11**, 111.
24 V. Demarne and A. Grisel, *Sens. Actuators, B*, 1993, **15–16**, 63.
25 S. Suh, Z. Zhang, W.-K. Chu and D. M. Hoffmann, *Thin Solid Films*, 1999, **345**, 240.
26 S. H. Park, Y. C. Son, W. S. Willis, S. L. Suib and K. E. Creasy, *Chem. Mater.*, 1998, **10**, 2389.
27 S. Shanthi, C. Subramanian and P. Ramasamy, *Mater. Sci. Eng., B*, 1999, **57**, 127.
28 E. Dien, J. M. Laurent and A. Smith, *J. Eur. Ceram. Soc.*, 1999, **19**, 787.
29 C. Nayral, T. Ould-Ely, A. Maisonnat, B. Chaudret, P. Fau, L. Lescouzère and A. Peyre-Lavigne, *Adv. Mater.*, 1999, **11**, 61.
30 T. Nutz and M. Haase, *J. Phys. Chem. B*, 2000, **104**, 8430.
31 C. Terrier, J.-P. Chatelon and J. A. Roger, *Thin Solid Films*, 1997, **295**, 95.
32 A. Gamard, O. Babot, B. Jousseaume, M. C. Rascle, T. Toupance and G. Campet, *Chem. Mater.*, 2000, **12**, 3419.
33 S. S. Park and J. D. Mackenzie, *Thin Solid Films*, 1996, **274**, 154.
34 A. Dieguez, A. Romano-Rodriguez, J. R. Morante, U. Weimar, M. Schweizer-Berberich and W. Göpel, *Sens. Actuators, B*, 1996, **31**, 1.
35 P. Siciliano, *Sensor Actuator B Chem*, 2000, **70**, 153.
36 M. I. Ivanovskaya, P. A. Bogdanov, D. R. Orlik, A. C. Gurlo and V. V. Romanovskaya, *Thin Solid Films*, 1997, **296**, 41.
37 S. G. Ansari, P. Boroojerdian, S. R. Sainkar, R. N. Karekar, R. C. Aiyer and S. K. Kulkarni, *Thin Solid Films*, 1997, **295**, 271.
38 S. H. Pulcinelli, C. V. Santilli, J. P. Jolivet and E. Tronc, *J. Non-Cryst. Solids*, 1994, **170**, 21.
39 G. E. S. Brito, S. J. L. Ribeiro, V. Briois, J. Dexpert-Ghys, C. V. Santilli and S. H. Pulcinelli, *J. Sol-Gel Sci. Technol.*, 1997, **8**, 261.
40 D. P. Tunstall, S. Patou, R. S. Liu and Y. H. Kao, *Mater. Res. Bull.*, 1999, **34**, 1513.
41 P. G. Harrison and A. Guest, *J. Chem. Soc., Faraday Trans.*, 1987, **83**, 3383.
42 L. Armelao, F. Ribot, and C. Sanchez, in *Better Ceramics Through Chemistry VII*, ed. B. Coltrain, C. Sanchez, D. W. Schaefer and G. L. Wilkes, Materials Research Society, Pittsburgh, PA, 1996, p. 387.
43 E. Scolan and C. Sanchez, *Chem. Mater.*, 1998, **10**, 3217.
44 M. Chatry, M. Henry, M. In, C. Sanchez and J. Livage, *J. Sol-Gel Sci. Technol.*, 1994, **1**, 233.
45 L. Broussous, C. V. Santilli, S. H. Pulcinelli and A. F. Craievich, *J. Phys. Chem.*, 2002, **106**, 2855.
46 V. Peyre, O. Spalla, L. Belloni and M. Nabavi, *J. Colloid Interface Sci.*, 1997, **187**, 184.
47 C. J. Brinker and G. W. Scherer, *Sol-Gel Science: The Physics and Chemistry of Sol-Gel Processing*, Academic Press, San Diego, CA, 1990.
48 J.-P. Jolivet, *Metal Oxide Chemistry and Synthesis: from Solution to Solid State*, Wiley-VCH, Weinheim, 2000.
49 M. Kallala, C. Sanchez and B. Cabane, *Phys. Rev. E.*, 1993, **48**, 3692.
50 J. C. Debsikbar, *J. Non-Cryst. Solids*, 1986, **87**, 343.
51 C. Sanchez, J. Livage, M. Henry and F. Babonneau, *J. Non-Cryst. Solids*, 1988, **100**, 65.
52 P. Papet, N. Lebars, J. F. Baumard, A. Lecomte and A. Dauger, *J. Mater. Sci.*, 1989, **24**, 3850.
53 F. Ribot, P. Toledano and C. Sanchez, *Chem. Mater.*, 1991, **3**, 759.
54 J. Blanchard, S. Barboux-Doeuff, J. Maquet and C. Sanchez, *New J. Chem.*, 1995, **19**, 929.
55 A. Gamard, B. Jousseaume, T. Toupance and G. Campet, *Inorg. Chem.*, 1999, **38**, 4671.
56 J. Blanchard, F. Ribot, C. Sanchez, P.-V. Bellot and A. Trokiner, *J. Non-Cryst. Solids*, 2000, **265**, 83.
57 A. Guinier, *Théorie et Technique de la Radiocristallographie*, Dunod, Paris, 1964.
58 H. Reuter and A. Sebald, *Z. Naturforsch., B*, 1992, **48**, 195.
59 D. Massiot, H. Thiele and A. Germanus, *Bruker Report*, 1994, **140**, 43.
60 C. D. Chandler, A. D. Fallon, A. J. Koplick and B. O. West, *Aust. J. Chem.*, 1987, **40**, 1427.
61 R. C. Mehrotra, R. Bohra and D. P. Gaur, *Metal β-Diketonates and Allied Derivatives*, Academic Press, London, 1978.
62 M. J. Hampden-Smith, T. A. Wark and C. J. Brinker, *Coord. Chem. Rev.*, 1992, **112**, 81.
63 Powder Diffraction File no. 41-1445, JCPDS, International Center for Diffraction Data, Swarthmore, PA, USA, 1993.
64 K. Nakamoto, *Infrared and Raman Spectra of Inorganic and Coordination Compounds*, Wiley, New York, 1978.
65 A. Novak, *Struct. Bonding*, 1974, **18**, 177.
66 C. Cossement, J. Darville, J.-M. Gilles, J. B. Nagy, C. Fernandez and J.-P. Amoureux, *Magn. Reson. Chem.*, 1992, **30**, 263.